Eur. Phys. J. B **16**, 209–212 (2000)

THE EUROPEAN PHYSICAL JOURNAL B
EDP Sciences

Rapid Note

Single hole dynamics in the one-dimensional t-J model

M. Brunner[a], F.F. Assaad, and A. Muramatsu

Institut für Theoretische Physik III, Universität Stuttgart, Pfaffenwaldring 57, 70550 Stuttgart, Germany

Received 15 February 2000

Abstract. We present a new finite-temperature quantum Monte Carlo algorithm to compute imaginary-time Green functions for a single hole in the t-J model on non-frustrated lattices. Spectral functions are obtained with the Maximum Entropy method. Simulations of the one-dimensional case show that a simple charge-spin separation *Ansatz* is able to describe the overall features of the spectral function such as the bandwidth $W \sim 4t + J$ and the compact support of the spectral function, over the whole energy range for values of J/t from 1/3 to 4. This is contrasted with the two-dimensional case. The quasiparticle weight Z_k is computed on lattices up to $L = 128$ sites in one dimension, and scales as $Z_k \propto L^{-1/2}$.

PACS. 71.10.Fd Lattice fermion models (Hubbard model, etc.) – 71.10.Pm Fermions in reduced dimensions (anyons, composite fermions, Luttinger liquid, etc.)

Understanding single hole dynamics in quantum antiferromagnets is a decisive step towards a comprehensive description of elementary excitations in strongly correlated systems. After the pioneering work by Brinkman and Rice [1], where the propagation of a hole is studied neglecting quantum fluctuations of the spin background, an enormous amount of theoretical work developed in the last decade on the subject mainly due to high temperature superconductors [2]. This interest was revived again by recent experimental realizations in compounds such as $SrCuO_2$ [3], $Na_{0.96}V_2O_5$ [4] for chains, $Sr_{14}Cu_{24}O_{41}$ [5] for ladders and $Sr_2CuO_2Cl_2$ [6] for planes. In particular chain compounds attract at present an increasing amount of interest in order to elucidate, whether signals of charge-spin separation as predicted from Luttinger-liquid theory [7,8] can be observed experimentally. On the other hand, theoretical treatments based on Bethe-*Ansatz* (BA) results led recently to a complete description of the spectral function of the Hubbard model at $U = \infty$ [9] and the low energy sector in the nearest-neighbour (NN) t-J model, where explicit results are obtained at the supersymmetric (SuSy) point [10]. Further exact results – apart from exact diagonalizations which suffer from strong finite-size effects – are available only for the inverse-square exchange (ISE) [11] t-J model at the SuSy point. In order to be able to compare with experiments, it is crucial to extend such studies to realistic values of the parameters and possibly beyond the asymptotic low energy limit.

In this paper, we present a simple finite-temperature quantum Monte Carlo (QMC) algorithm capable of dealing with this issue for the NN t-J model. For single-hole excitations and in the absence of frustration, the method is free of the notorious sign problem, and applicable to chains, n-leg ladders and planes. Here, we concentrate predominately on chains. Our simulations lead to the conclusion that the overall features of the spectral functions are well described by a charge-spin separation *Ansatz* (CSSA) based on a mean-field slave-boson picture [12], where the hole spectral function is given by the convolution of the spectral functions of free holons and spinons. The agreement with the simulations is obtained over all energy scales and values of J/t ranging from 1/3 to 4, thus showing the applicability of a simple phenomenological model to describe hole-dynamics in one dimension. At the SuSy point a more detailed understanding of the spectrum is achieved by supplementing the simple model with BA results. A finite-size scaling on chains up to $L = 128$ sites shows that the quasiparticle weight Z_k vanishes as $1/\sqrt{L}$, a result which was beyond numerical capabilities up to now.

Our starting point is the NN t-J model,

$$H_{t-J} = -t \sum_{\langle i,j\rangle,\sigma} \tilde{c}^\dagger_{i,\sigma}\tilde{c}_{j,\sigma} + J \sum_{\langle i,j\rangle} \left(\mathbf{S}_i \cdot \mathbf{S}_j - \frac{1}{4}\tilde{n}_i\tilde{n}_j \right). \quad (1)$$

Here $\tilde{c}^\dagger_{i,\sigma}$ are projected fermion operators $\tilde{c}^\dagger_{i,\sigma} = (1 - c^\dagger_{i,-\sigma}c_{i,-\sigma})c^\dagger_{i,\sigma}$, $\tilde{n}_i = \sum_\alpha \tilde{c}^\dagger_{i,\alpha}\tilde{c}_{i,\alpha}$, $\mathbf{S}_i = (1/2)\sum_{\alpha,\beta} c^\dagger_{i,\alpha}\sigma_{\alpha,\beta}c_{i,\beta}$, and the sum runs over nearest neighbours. After a canonical transformation this model is cast into the form [13]

$$\tilde{H}_{t-J} = +t \sum_{\langle i,j\rangle} P_{ij} f^\dagger_i f_j + \frac{J}{2} \sum_{\langle i,j\rangle} \Delta_{ij}(P_{ij} - 1), \quad (2)$$

where $P_{ij} = (1 + \boldsymbol{\sigma}_i \cdot \boldsymbol{\sigma}_j)/2$, $\Delta_{ij} = (1 - n_i - n_j)$ and $n_i = f^\dagger_i f_i$. In this mapping, one uses the following identities for the standard creation ($c^\dagger_{i,\sigma}$) and annihilation ($c_{i,\sigma}$)

[a] e-mail: michi@theo3.physik.uni-stuttgart.de

operators $c_{i\uparrow}^{\dagger} = \gamma_{i,+} f_i - \gamma_{i,-} f_i^{\dagger}$, $c_{i\downarrow}^{\dagger} = \sigma_{i,-}(f_i + f_i^{\dagger})$, where $\gamma_{i,\pm} = (1 \pm \sigma_{i,z})/2$ and $\sigma_{i,\pm} = (\sigma_{i,x} \pm i\sigma_{i,y})/2$. The spinless fermion operators fulfill the canonical anticommutation relations $\{f_i^{\dagger}, f_j\} = \delta_{i,j}$, and $\sigma_{i,a}$, $a = x, y$, or z are the Pauli matrices. The constraint to avoid doubly occupied states transforms to the conserved and holonomic constraint $\sum_i \gamma_{i,-} f_i^{\dagger} f_i = 0$.

The Green function in the spin up sector may be written as

$$G_{\uparrow}(i-j,\tau) = \langle T\tilde{c}_{i,\uparrow}(\tau)\tilde{c}_{j,\uparrow}^{\dagger}\rangle = \langle T f_i^{\dagger}(\tau) f_j\rangle \tag{3}$$

where T is the time ordering operator. Inserting complete sets of spin states we obtain

$$\begin{aligned} -G(i-j,-\tau) &= \frac{\sum_{\sigma_1}\langle v|\otimes\langle\sigma_1|\mathrm{e}^{-(\beta-\tau)\tilde{H}_{t-J}} f_j \mathrm{e}^{-\tau\tilde{H}_{t-J}} f_i^{\dagger}|\sigma_1\rangle\otimes|v\rangle}{\sum_{\sigma_1}\langle\sigma_1|\mathrm{e}^{-\beta\tilde{H}_{t-J}}|\sigma_1\rangle} \\ &= \sum_{\boldsymbol{\sigma}} P(\boldsymbol{\sigma}) \\ &\times \frac{\langle v|f_j \mathrm{e}^{-\Delta\tau\tilde{H}(\sigma_n,\sigma_{n-1})}\mathrm{e}^{-\Delta\tau\tilde{H}(\sigma_{n-1},\sigma_{n-2})}\ldots\mathrm{e}^{-\Delta\tau\tilde{H}(\sigma_2,\sigma_1)} f_i^{\dagger}|v\rangle}{\langle\sigma_n|\mathrm{e}^{-\Delta\tau\tilde{H}_{t-J}}|\sigma_{n-1}\rangle\ldots\langle\sigma_2\mathrm{e}^{-\Delta\tau\tilde{H}_{t-J}}|\sigma_1\rangle} \\ &+\mathcal{O}(\Delta\tau^2) = \sum_{\boldsymbol{\sigma}} P(\boldsymbol{\sigma}) G(i,j,\tau,\boldsymbol{\sigma}) + \mathcal{O}(\Delta\tau^2). \end{aligned} \tag{4}$$

Here $m\Delta\tau = \beta$, $n\Delta\tau = \tau$, $\Delta\tau t \ll 1$ and $\exp(-\Delta\tau\tilde{H}(\sigma_1,\sigma_2))$ is the evolution operator for the holes, given the spin configuration (σ_1,σ_2). In the case of single hole dynamics $|v\rangle$ is the vacuum state for holes, and $P(\boldsymbol{\sigma})$ is the probability distribution of a Heisenberg antiferromagnet for the configuration $\boldsymbol{\sigma}$, where $\boldsymbol{\sigma}$ is a vector containing all intermediate states $(\sigma_1,\ldots\sigma_n,\ldots\sigma_m,\sigma_1)$. The sum over spins is performed in a very efficient way by using a world-line cluster-algorithm [14]. As the evolution operator for the holes is a bilinear form in the fermion operators, $G(x,\tau,\boldsymbol{\sigma})$ can be calculated exactly in contrast to the worm approach [15], where fermion paths are sampled stochastically. The numerical effort to calculate $G(x,\tau,\boldsymbol{\sigma})\ \forall x,\tau$ scales as $L\tau$. Spectral properties are obtained by inverting the spectral theorem

$$G(k,\tau) = \int_{-\infty}^{\infty} \mathrm{d}\omega\ A(k,\omega)\frac{\exp(-\tau\omega)}{\pi(1+\exp(-\beta\omega))} \tag{5}$$

with the Maximum Entropy method (MEM) [16]. Since $P(\boldsymbol{\sigma})$ is the probability distribution for the quantum antiferromagnet, the algorithm does not suffer from sign problems on bipartite lattices and next neighbour interactions in any dimension. However, when the spin and charge dynamics evolve according to very different time scales ($J \lesssim 0.2t$), $G(x,\tau,\boldsymbol{\sigma})$ shows an increasing variance. Best results are obtained at the SuSy point and an appreciable range of J/t may be considered as shown below.

We now concentrate on the one-dimensional t-J model. The simulations were performed at temperatures $T \leq \min(J,t)/15$, such that no appreciable changes with a further decrease in temperature can be seen: the results correspond to the zero temperature limit, a limit which is in general difficult to reach in other finite-temperature fermionic algorithms. For the MEM we use a flat default model without prior knowledge and covariance of the data. We checked the reliability of our MEM results by adding white noise within the error bars to our data. We find no relevant changes on the results. For the worst case, the lower edge of the support and the upper edge around $k = 0$ have a root-mean-square deviation of less than $0.05\omega/t$. For the upper edge the deviation grows to approximately $0.4\omega/t$ for larger values of k.

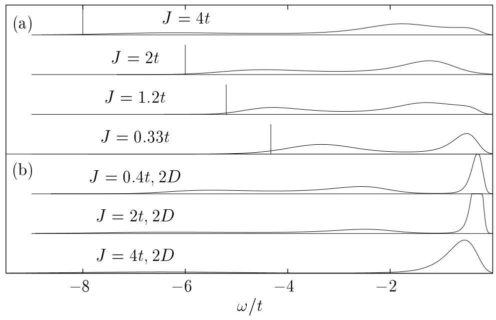

Fig. 1. Density of states $N(\omega)$ for different values of J/t in (a) 1D for a 64 site chain and (b) 2D for a 16×16 lattice. The vertical line in (a) indicates $4t + J$.

We compare our results with the predictions of the CSSA, where free holons and spinons are described by [12,17]

$$H = -\frac{t_h}{2}\sum_{\langle i,j\rangle} h_i^{\dagger} h_j - \frac{J_s}{2}\sum_{\langle i,j\rangle} s_{i,\sigma}^{\dagger} s_{j,\sigma}. \tag{6}$$

Here the electron operator $c_{i,\sigma}$ is given by the product of a holon (h_i) and a spinon ($s_{i,\sigma}$) operator, $c_{i\sigma} = s_{i,\sigma} h_i^{\dagger}$, the holon being a boson and the spinon a spin-1/2 fermion. As a consequence of the above *Ansatz*, the dispersion relations of the free holons and spinons are given by $\epsilon_{\mathrm{h}} = -t_{\mathrm{h}}\cos q_{\mathrm{h}}$ and $\epsilon_{\mathrm{s}} = -J_{\mathrm{s}}\cos q_{\mathrm{s}}$ respectively, whereas the energy of the hole is $E(k) = \epsilon_{\mathrm{h}} - \epsilon_{\mathrm{s}}$ and by momentum conservation $k = q_{\mathrm{h}} - q_{\mathrm{s}}$. We take t_{h} and J_{s} as two free parameters in contrast to a mean-field approximation, where they have to be calculated self-consistently. The spectral function is then given by a convolution of the spinon and holon Green functions. The lowest attainable energy ($-t_{\mathrm{h}}$) and highest one ($t_{\mathrm{h}} + J_{\mathrm{s}}$) define the bandwidth of the hole, $2t_{\mathrm{h}} + J_{\mathrm{s}}$. Since the full bandwidth obtained by considering the compact support of the spectral function at $J = 0$ is known to be exactly $4t$ [9], we take $t_{\mathrm{h}} = 2t$. In order to determine J_{s}, we consider the overall bandwidth, as obtained from the simulation. As can be seen in Figure 1a, for all values of J, the width of the density of states $N(\omega)$ scales approximately as $4t + J$ in the parameter range considered, leading to $J_{\mathrm{s}} = J$. Instead, the results in two dimensions (2D) (Fig. 1b) show no appreciable change of the bandwidth for $0.4t \leq J \leq 4t$. On increasing J, weight is just transferred to the low-energy peak that results from extremely flat bands around $\mathbf{k} = (\pi, 0)$ [18–20]. The results for $J = 0.4t$ are in very good agreement with previous exact diagonalizations [18]. A complete account of the 2D case will be published elsewhere.

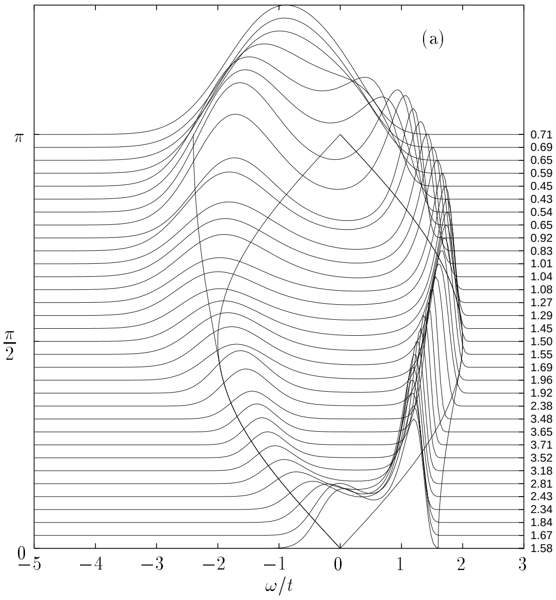

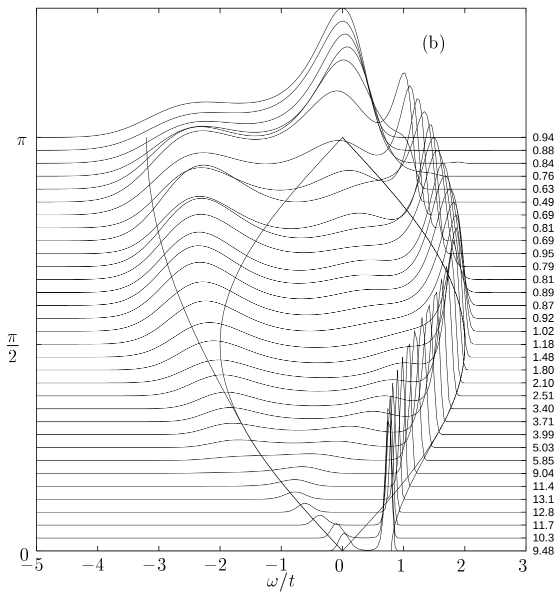

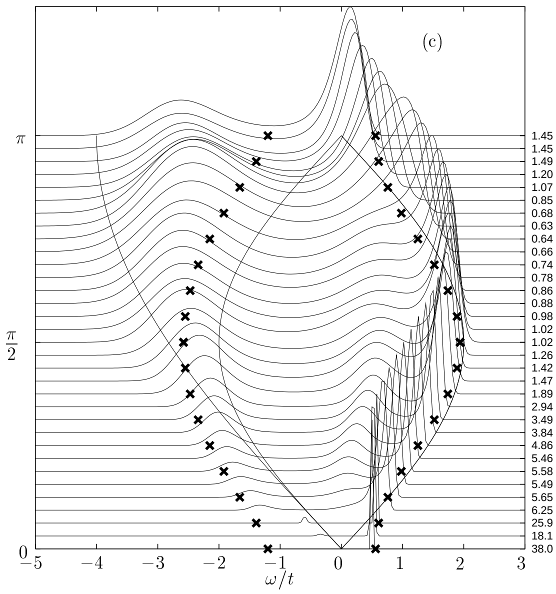

Fig. 2. Spectral function $A(k, \omega)$ for (a) $J = 0.4t$, (b) $J = 1.2t$, and (c) $J = 2t$ on a 64 site chain. Here the wave vector $k \in [0, \pi]$ is given on the y-axis. For clarity, the data is rescaled by the number given at the right hand side of the plot. Further details are discussed in the text.

Beyond predicting bandwidths, the CSSA in 1D describes accurately the support of the spectral function in the case $J = 0$, when compared with exact results [9,12]. If furthermore phase string effects [12] are taken into account, the singularities of $A(k, \omega)$ related to holons and spinons can be reproduced. For finite J, the minimal (maximal) possible energy of a hole in CSSA is given by $E(k) = -F_k$ ($E(k) = F_k$) for $k < k_0$ ($k > k_0$), where $F_k \equiv \sqrt{J^2 + 4t^2 - 4tJ\cos(k)}$ contains both holon and spinon contributions, and k_0 is determined by $\cos(k_0) = J/(2t)$. The remaining parts of the compact support are given by $E(k) = \mp 2t\sin(k)$ for $k > k_0$ (lower edge) and $k < k_0$ (upper edge) respectively. Such dispersions correspond to holons with momentum $k + q_s$, and a spinon with $q_s = \mp\pi/2$ [10,12]. As $J \to 2t$, $k_0 \to 0$ and the lower edge of the compact support is entirely determined by the dispersion of the holon.

We now compare the above predictions with our QMC data. Figure 2 shows $A(k, \omega)$ for $J/t = 0.4$ (a), 1.2 (b) and 2 (c). In all cases the compact support is reproduced very well by the CSSA. The *Ansatz* also predicts singularities at the lower (upper) edge for $k < k_0$ ($k > k_0$), and when phase strings are considered [12] along the edges and the holon lines ($\pm 2t\sin(k)$) for all momenta. The singularities along the lower holon line were predicted in Luttinger-liquid theory [7,8], and for $U = \infty$ in the Hubbard model [9]. They are also supported by a recent low energy theory [10]. For all parameter values we observe dominant weight along the above mentioned lines. For $J/t = 0.4$, we have checked that the results are consistent within the uncertainties of MEM with a peak along the edges and a further peak along the holon lines, signaled by a broad structure between the edges and the holon lines (Fig. 2a). We observed such a behaviour for $0.33 \le J/t \le 0.6$. For $J/t \ge 1.2$ (Figs. 2b and c), the structure at the lower edge narrows considerably and the data are not any more consistent with an additional structure along the lower holon line for $k < k_0$, but only with

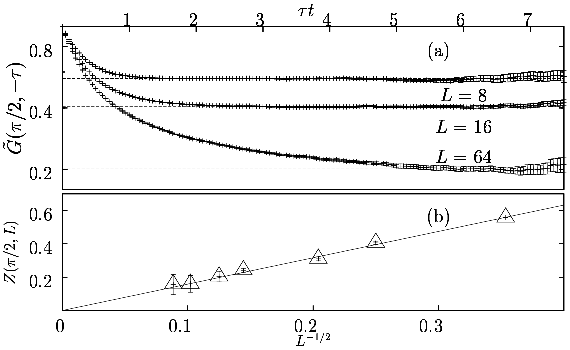

Fig. 3. Quasiparticle weight at $k = \pi/2$. (a) $\tilde{G}(\pi/2,-\tau) \equiv G(\pi/2,-\tau)\,\exp\left[-\tau\left(E_0^L - E_0^{L-1}(\pi/2)\right)\right]$ *versus* τ/t. At $\tau/t \gg 1$ this quantity converges to the quasiparticle weight $Z(\pi/2)$. (b) Finite size scaling of $Z(\pi/2)$ as obtained from (a). The solid line is a least square fit to the form $L^{-1/2}$. We consider $\beta J = 30$ for $L \le 48$, $\beta J = 60$ for $96 \ge L > 48$, and $\beta J = 90$ for $L = 128$, to guarantee convergence in τ.

a singularity for $k > k_0$. At $J/t = 2$ the exact holon and spinon dispersions can be obtained by BA [21]. Figure 2c shows the comparison with the CSSA, where on the one side the original dispersions are used (full line) and on the other side, with the dispersions as given by BA (crosses). Whereas the BA holon dispersion reproduces very well the lower edge, showing that as anticipated by the CSSA, at the SuSy point that edge is completely determined by the holon dispersion, the full bandwidth is better described with the original dispersions. We assign the additional weight in the region $k > \pi/2$ to processes involving one holon and more than one BA spinon. In fact, that portion resembles the difference between the supports for one-holon/one-spinon and one-holon/three-spinon processes in the ISE model [11]. In our case, no limitation on the possible number of spinons exists, such that in principle all odd numbers of them are allowed. It is interesting to notice that using a fermionic spinon one is able to describe both the case $J = 0$ and $J = 2t$. In the first case, the spinon in the exact solution is a fermion. At the SuSy point it is expected to be a semion [11,22] and on the basis of our results, we conclude that the fermionic spinon contains all possible states with an odd number of semionic spinons.

Finally, we consider the quasiparticle residue $Z_k = \left|\langle \Psi_0^{L-1} | \tilde{c}_{k\sigma} | \Psi_0^L \rangle\right|^2$ at $k = \pi/2$ for $J = 2t$. As Figure 2c shows, the lower edge is very sharp and without prior knowledge, the question may arise whether we are dealing with a quasiparticle. Z_k is related to the imaginary time Green function through:

$$\lim_{\tau \to \infty} G(k,-\tau) \propto Z_k \exp\left[\tau\left(E_0^L - E_0^{L-1}(k)\right)\right]. \quad (7)$$

Figure 3a shows $G(\pi/2,-\tau)\exp\left(-\tau(E_0^L - E_0^{L-1}(\pi/2))\right)$ *versus* τ, where the energy difference is obtained by fitting the tail of $G(\pi/2,-\tau)$ to a single exponential form, for several sizes. The thus estimated $Z(\pi/2)$ is plotted *versus* system size in Figure 3b. Our results are consistent with a vanishing quasiparticle weight $Z(\pi/2) \propto L^{-1/2}$ which is the scaling obtained by a combination of bosonization and conformal field theory [10]. Since the CPU-times scales as $V\beta$ (V is the volume) the determination of the Z-factor may be efficiently extended to higher dimensions, in contrast to determinantal algorithms for the Hubbard model that scale as $V^3\beta$.

In summary, we have developed a new QMC algorithm which allows the determination of single-hole dynamics in quantum antiferromagnets. This algorithm is extremely powerful in the sense, that the required CPU time scales as $V\beta$. For the one dimensional case, we showed that the spectral function is well described by a simple model with free spinons and holons with dispersions given by J and $2t$. This is not the case in 2D. The comparison of our results at the supersymmetric point lead to a characterization of the excitation content of the spectra for this particular parameter, where additional information is available from the Bethe *Ansatz* solution. Finally we computed the quasiparticle weight and showed that it vanishes as $L^{-1/2}$.

This work was supported by Sonderforschungsbereich 382. The numerical calculations were performed at HLRS Stuttgart and HLRZ Jülich. We thank the above institutions for their support.

References

1. W.F. Brinkman, T.M. Rice, Phys. Rev. B **2**, 1324 (1970).
2. E. Dagotto, Rev. Mod. Phys. **66**, 763 (1994).
3. C. Kim *et al.*, Phys. Rev. Lett. **77**, 4054 (1996).
4. K. Kobayashi *et al.*, Phys. Rev. Lett. **82**, 803 (1999).
5. T. Takahashi *et al.*, Phy. Rev. B **56**, 7870 (1997).
6. B.O. Wells *et al.*, Phys. Rev. Lett. **74**, 964 (1995).
7. V. Meden, K. Schönhammer, Phys. Rev. B **46**, 15753 (1992); K. Schönhammer, V. Meden, *ibid.* **47**, 16205 (1993).
8. J. Voit, Rep. Prog. Phys. **58**, 977 (1995).
9. S. Sorella, A. Parola, J. Phys. Cond. Matter **4**, 3589 (1992); K. Penc, F. Mila, H. Shiba, Phys. Rev. Lett. **75**, 894 (1995).
10. S. Sorella, A. Parola, Phys. Rev. Lett. **76**, 4604 (1996); Phys. Rev. B **57**, 6444 (1998).
11. Y. Kato, Phys. Rev. Lett. **81**, 5402 (1998); A.N.C. Ha, F.D.M. Haldane, Phys. Rev. Lett. **73**, 2887 (1994).
12. H. Suzuura, N. Nagaosa, Phys. Rev. B **56**, 3548 (1997).
13. G. Khaliullin, JETP Lett. **52**, 389 (1990); A. Angelucci, Phys. Rev. B **51**, 11580 (1995).
14. H.G. Evertz, M. Marcu, G. Lana, Phys. Rev. Lett. **70**, 875 (1993).
15. N.V. Prokof'ev, B.V. Svistunov, I.S. Tupitsyn, JETP **87**, 310 (1998).
16. M. Jarrell, J. Gubernatis, Phys. Rep. **269**, 133 (1996); W. von der Linden, Appl. Phys. A **60**, 155 (1995).
17. P.W. Anderson, Science **235**, 1196 (1987); G. Baskaran, P.W. Anderson, Phys. Rev. B **37**, 580 (1988).
18. K.J. von Szczepanski, P. Horsch, W. Stephan, M. Ziegler, Phys. Rev. B **41**, 2017 (1990).
19. M. Boninsegni, Phys. Lett. A **199**, 330 (1994).
20. F.F. Assaad, M. Imada, Eur. Phys. J. B **10**, 595 (1999).
21. P.-A. Bares, G. Blatter, Phys. Rev. Lett. **64**, 2567 (1990); P.-A. Bares, G. Blatter, M. Ogata, Phys. Rev. B **44**, 130 (1991).
22. F.D.M. Haldane, in *Correlation Effects in Low-Dimensional Electron Systems*, edited by A. Okiji, N. Kawakami (Springer Verlag, Berlin, 1994).